ORIGINAL PAPER

Voltammetric biosensor for coronavirus spike protein using magnetic bead and screen-printed electrode for point-of-care diagnostics

Pravanjan Malla[1] · Hao-Ping Liao[1] · Chi-Hsien Liu[1,2,3,4] · Wei-Chi Wu[4,5] · Paiboon Sreearunothai[6]

Abstract

The rapid spread of the novel human coronavirus 2019 (COVID-19) and its morbidity have created an urgent need for rapid and sensitive diagnostics. The real-time polymerase chain reaction is the gold standard for detecting the coronavirus in various types of biological specimens. However, this technique is time consuming, labor intensive, and expensive. Screen-printed electrodes (SPEs) can be used as point-of-care devices because of their low cost, sensitivity, selectivity, and ability to be miniaturized. The ability to detect the spike protein of COVID-19 in serum, urine, and saliva was developed using SPE aided by magnetic beads (MBs) and a portable potentiostat. The antibody-peroxidase-loaded MBs were the captured and catalytic units for the electrochemical assays. The MBs enable simple washing and homogenous deposition on the working electrode using a magnet. The assembly of the immunological MBs and the electrochemical system increases the measuring sensitivity and speed. The physical and electrochemical properties of the layer-by-layer modified MBs were systematically characterized. The performance of these immunosensors was evaluated using spike protein in the range 3.12–200 ng mL^{-1}. We achieved a limit of detection of 0.20, 0.31, and 0.54 ng mL^{-1} in human saliva, urine, and serum, respectively. A facile electrochemical method to detect COVID-19 spike protein was developed for quick point-of-care testing.

Keywords COVID-19 · Spike protein · Screen-printed electrodes · Magnetic beads

Pravanjan Malla and Hao-Ping Liao contributed equally to this work.

✉ Chi-Hsien Liu
CHL@mail.cgu.edu.tw

[1] Department of Chemical and Materials Engineering, Chang Gung University, 259, Wen-Hwa First Road, Taoyuan, Taiwan

[2] Research Center for Chinese Herbal Medicine and Research Center for Food and Cosmetic Safety, College of Human Ecology, Chang Gung University of Science and Technology, 261, Wen-Hwa First Road, Taoyuan, Taiwan

[3] Department of Chemical Engineering, Ming Chi University of Technology, 84, Gung-Juan Road, New Taipei City, Taiwan

[4] Department of Ophthalmology, Chang Gung Memorial Hospital, Linkou, 5, Fu-Hsing Street, Taoyuan, Taiwan

[5] College of Medicine, Chang Gung University, 259, Wen-Hwa First Road, Taoyuan, Taiwan

[6] Sirindhorn International Institute of Technology, Thammasat University, Pathum Thani, Thailand

Introduction

The rapid spread of the novel human coronavirus 2019 (COVID-19) and its morbidity have created an urgent need for rapid and sensitive diagnostics. Conventional methods for virus detection include lateral flow strips, enzyme-linked immunosorbent assay, and polymerase chain reaction (PCR) [1]. Among these techniques, PCR is the gold standard for detecting coronaviruses from various types of biological specimens. The main drawbacks of thermal cyclers include long analysis time, expensive instrument setup, and the need for skilled personnel [2]. Various virus detection methods, including electrochemical biosensors, fluorescence biosensors, surface-enhanced Raman scattering-based biosensors, colorimetric biosensors, chemiluminescence biosensors, surface plasmon resonance-based biosensors, and magnetic biosensors, have been developed for SARS-CoV-2 [3]. Among these detection principles, electrochemical biosensors can consist of potentiometric, amperometric, conductometric, voltammetric, polarographic, impedimetric, capacitive, or piezoelectric elements [4]. Moreover, biosensors incorporated with different recognition elements such as imprinted

polymers, enzymes, antibodies, DNA, and aptamers can be applied for virus detection [5]. These excellent reviews have summarized the background of the principles and mechanisms for virus detection using biosensors.

Electrochemical biosensors can be used as point-of-care devices because of their low cost, selectivity, and ability to be miniaturized [6]. Electrochemical biosensors to detect SARS-CoV-2, such as screen-printed electrodes (SPEs) and field-effect transistors (FET), also have been widely used [7]. The electrochemical sensing of coronavirus amplicons from PCR has been developed using printed-circuit-board (PCB) electrodes [8]. In addition, SPEs have advantages such as easy production, low cost, disposability, sensitivity, and miniaturization [9, 10]. Ehsan et al. chose SPEs as impedance immunosensors to detect coronavirus in nasopharyngeal fluid samples. Antibody immobilization on a carbon electrode provides a low limit of quantification (0.25 fg mL^{-1}) of patients' samples [11]. SPEs coated with gold nanoparticles are applied to immobilize antibodies against the coronavirus nucleocapsid with a linear range from 1.0 pg mL^{-1} to 100 ng mL^{-1} and a limit of detection of 0.4 pg mL^{-1} [12]. The Cu$_2$O-modified SPE is used to detect the spike protein of SARS-CoV-2 using charge transfer resistance. The assay range is around 0.25 fg mL^{-1} to 1 µg mL^{-1} within 20 min, and it exhibits a recovery rate of ~97–103% in different artificial saliva, artificial nasal, and universal transport media [13]. These studies indicate the potential and power of disposable electrochemical biosensors. However, these studies must also address the issues of complex manufacturing and the time needed for analysis if they are to be applicable for point-of-care testing.

Magnetic beads (MB) integrated with SPE have been applied to detect different biomarkers [14, 15]. In this study, the facile detection of spike protein in serum, urine, and saliva was developed using MB-based disposable SPE in combination with a portable potentiostat. The antibody-peroxidase-loaded MBs are the detection platform for electrochemical assays. The MBs enable simple washing and easy separation on the working electrode using a magnet. The assembly of the MBs and enzymatic reaction on the electrode surface can increase the measurement sensitivity. The electrochemical signal is generated by peroxidase using hydrogen peroxide and hydroquinone as the substrates. We systematically characterized the platform of MBs and SPEs by scanning electron microscopy (SEM), thermogravimetric analysis (TGA), and a superconducting quantum interference device (SQUID). The performance of these immunosensors was evaluated using square wave voltammetry (SWV) to detect spike protein added to saliva, urine, and serum.

Experimental

Reagents and materials

MB-NH$_2$ and MB-COOH (U-108, U-118) were purchased from TAN Bead (Taoyuan, Taiwan). Hydroquinone (HQ), glutaraldehyde, sodium phosphate dibasic, sodium phosphate monobasic, 3-aminophenyl boronic acid hemi sulfate salt (APBA, 95%), polyethylene glycol (PEG, mw:3350), dextran sulfate (DS), glucose, bovine serum albumin (BSA), vitamin C, and human serum were from Sigma-Aldrich (MO, USA). DMEM was purchased from Elabscience (TX, USA). Urea was from J.T. Baker (Leicestershire, UK) and γ-cyclodextrin (γ-CD) was from Wako (Tokyo, Japan). DNase was from Worthington Co. (Lakewood, USA), and RNase was from GenMark (Taipei, Taiwan). Biotinylated detection antibody for SARS-COV-2 spike protein (S2) (Lot#0,918,201,221), streptavidin-HRP (Lot#G01152188), standard spike protein (Lot#C07152088), and ELISA kit were obtained from RayBio (GA, USA). Hydrogen peroxide (H$_2$O$_2$, 30%) was from Fluka (MI, USA). All other chemicals were of extra pure analytical grade and used without further purification. Phosphate buffer solution (0.1 M and pH 7.0) was the diluent to study the reactions. Water was freshly prepared using the ultrapure water system (Sartorius Lab instruments GmbH & Co, Gottingen, Germany). SPEs containing a counter, working, and Ag reference electrodes were from Zensor (TE-100, Taichung, Taiwan).

Apparatus

The morphology and size of modified MBs were characterized using a scanning electron microscope (SEM, HITACHI S-4700, Tokyo, Japan), transmission electron microscope (TEM, JM-1011, JEOL, Tokyo, Japan), and ZetaSizer® Nano ZS 90 (Malvern, Worcestershire, UK). The carbon-coated copper grid was used to load the nanomaterials for TEM analysis. Thermal decomposition of modified MBs was analyzed using Q50 Analyzer (TA Instruments, DE, USA) in a nitrogen environment at various heating rates. The electrochemical properties of the SPE were analyzed using a portable electrochemical simulator (Zensor, ECAS-100). All the UV spectra were recorded by a microplate reader (SpectroStar, BMG, Ortenberg, Germany).

Preparation of layer-by-layer modified MBs

A 100 µL aliquot of the MB-NH$_2$ was transferred into a 1.5 mL Eppendorf tube. The MBs were washed twice with 1 mL of 0.1 M phosphate buffer solution for 10 min, and the supernatant was discarded. Amine groups of MBs were

activated by 60 min continuous vortex in 100 μL of glutar-aldehyde (4×) solution. Then APBA was captured onto the activated beads for 60 min at 25 °C under continuous vortex. Separately, 100× biotin antibody and 100× of streptavidin-HRP were mixed in a tube and incubated for 45 min at 4 °C. The MB/APBA were washed twice with 0.1 M phosphate buffer solution, then 100 μL Ab-HRP solution was added to the MB/APBA and incubated for 30 min at 25 °C to form MB/APBA/Ab-HRP. Then, the MB/APBA/Ab-HRP was further blocked in 5% glucose (GLU) for 30 min. Subsequently, the MB/APBA/Ab-HRP/GLU was washed twice with 1 mL of 0.1 M phosphate buffer solution (pH 7.0). After the wash and separation, 100 μL spike protein in serum was added to MB/APBA/Ab-HRP/GLU and incubated for 30 min at room temperature.

Fabrication and assay of the MB-based immunosensor

The fabrication of the MB-based immunosensor is outlined in Fig. 1. First, an SPE was cleaned by sonication with DDW (10 s), and a neodymium magnet on the backside of the SPE was used to attract MB/APBA/Ab-HRP/GLU on the working electrode. Five microliters of modified MB (MB/APBA/Ab-HRP/GLU) was added to the SPE. The solution of 5.0/5.0 mM H_2O_2/HQ solution (95 μL) was added to the SPE surface and waited for 5 s for SWV measurement. SWV measurement of HRP signal on SPE was obtained by applying a potential range of -0.4~0.2 V in a H_2O_2/HQ solution as previously described [16].

Optimization of measuring parameters and signal definition

To optimize measurement, operation factors such as concentrations of antibody, HRP, H_2O_2/HQ, incubation time of antibody, reaction time of MBs were evaluated. Only one parameter was varied, and the other parameters were fixed. The SWV signal was obtained using 10 ng mL^{-1} serum spiked protein in this experiment. Each signal was repeated three times ($n=3$). Based on the signal/blank (S/B) ratio, the optimal parameters were selected. The S/B ratio was calculated using the previous definition [17, 18]:

$$S/B \text{ ratio} = \Delta I_{10}/\Delta I_0$$
$$\Delta I_0 = I_{PBS} - I_{HS}$$
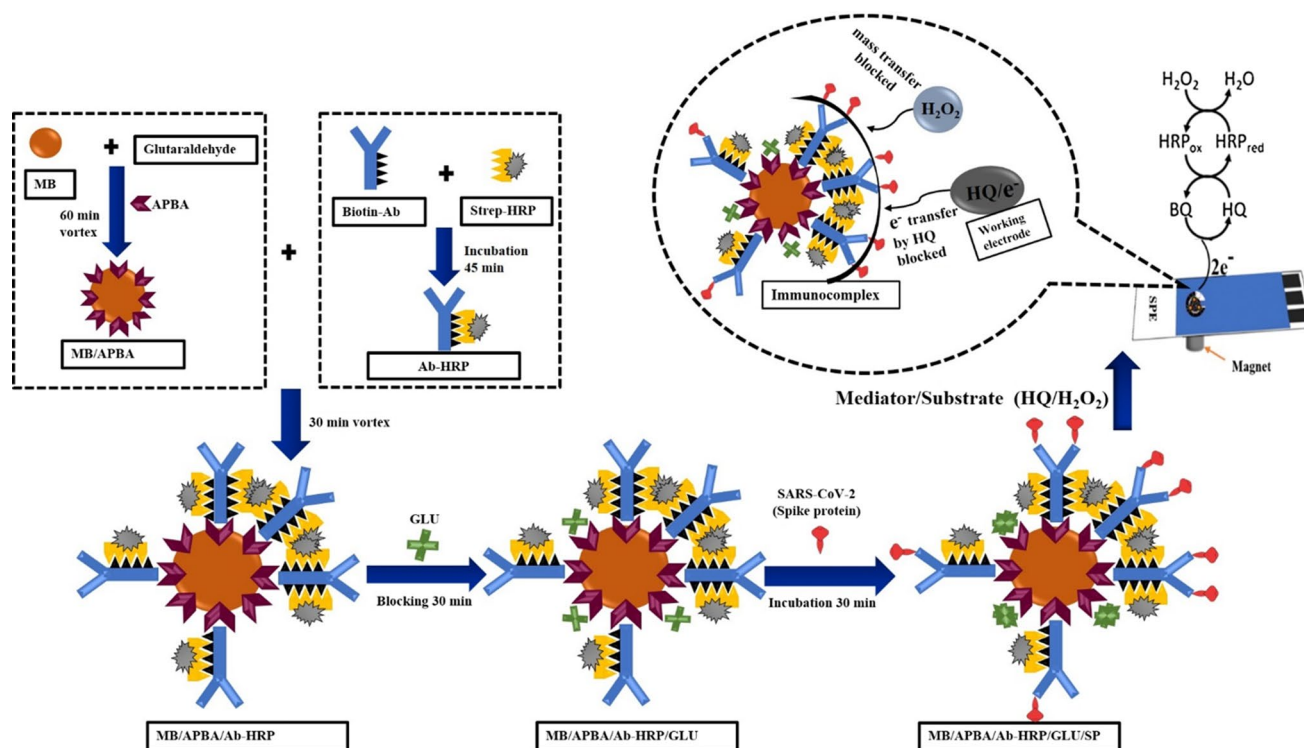$$\Delta I_{10} = I_{PBS} - I_{HS+\text{spike protein}}$$

Fig. 1 Schematic illustration for spike protein detection using the MB-based electrochemical immunosensor. MB/APBA/Ab-HRP/GLU/SP was synthesized using layer-by-layer modification. Ab-HRP was prepared by incubating a biotinylated antibody with streptavidin-HRP. 3-Aminophenyl boronic acid: APBA, glucose: GLU, spike pro-tein: SP. Ab-HRP binds preferentially to APBA on MB. Unbound APBA was blocked by GLU. Spike protein binds to Ab-HRP to form the immune complex, which can impede the substrate H_2O_2 and electron mediator HQ from reaching HRP's active site and electrode, and thus decrease in electrochemical signal

where I_{PBS} is the signal of MBs treated with phosphate buffer solution, I_{HS} is the signal of MBs treated in human serum without spike protein, $I_{HS + spike\ protein}$ is the signal of MBs treated with 10 ng mL^{-1} spike protein in human serum. The SWV signals of MBs were obtained using the 5.0 mM H_2O_2/5.0 mM HQ solution. The principle of the S/B calculation was demonstrated in Fig. S1.

SWV and EIS assay procedure

Cyclic voltammetry (CV) and electrochemical impedance spectroscopy (EIS) were used to study the different steps of immobilization, whereas the quantitative measurements were done using SWV. CV was cycled from -0.5 to 0.6 V with a scan rate of 50 mV s^{-1}. SWV was recorded from 200 to -400 mV with the increment time of 5 ms, amplitude of 75 mV, sample width of 6 ms, and pulse period of 100 ms. EIS was run with amplitude 100 mV, frequency range $1 \sim 1000$ Hz, and initial potential 20 mV. The real and imaginary components from impedance data of EIS were plotted as Nyquist plots. A semicircle in the Nyquist plot corresponds to the electron-transfer process, and the diameter of the semicircle is equal to the resistance of charge transfer (Rct). The EIS data of the modified MBs were also regressed by software (Zsimpwin) using the resistor–capacitor-resistor equivalent circuit to obtain the resistance and capacitance of the MB-loaded electrode. Histogram of charge transfer resistance and peak current of different MBs were studied. Assays were performed in triplicate, and the error bar represented the standard deviation of the measurement. The Ks by the CV method was evaluated using the Nicholson method as described previously [17].

Association constant analysis

In order to understand spike protein capture by the immobilized antibody on MBs, the association constant (Ka) for the binding between spike protein and the antibody was determined using EIS and the Langmuir isotherm assumptions such as monolayer adsorption and equal binding energy for all binding sites. θ represents the occupied ratio of antibody binding sites, and Ka is related to the equilibrium adsorption between spike protein and antibody on MBs. The Ka and θ were calculated using the Rct data from EIS as described previously [17].

Statistical analysis

In this study, all data are reported as means $\pm$ standard deviations (SD) in three repeats. The mean and SD of measurements were calculated using Microsoft Excel to evaluate the reproducibility. The data are expressed as mean $\pm$ standard deviation from three repeats. To predict the limit of detection

(LOD) and recovery rate (%), the following formulas were used [19]:

$$LOD = 3 \times \frac{SD}{m}$$

where SD is the standard deviation of the lowest concentration of spike protein and m is the slope of the calibration curve.

$$Recovery(\%) = \frac{found}{added} \times 100$$

Results and discussion

Principle of SARS-CoV-2 biosensor

The detection mechanism and fabrication steps of the developed MB-based immunosensor for the detection of COVID-19 spike protein are demonstrated in Fig. 1. Layer-by-layer modified MBs are used to fasten the assay through simultaneous capture and concentration of the targets with the aid of a magnet. The APBA modified MBs (MB/APBA) can immobilize Ab-HRP via diol-boronic ester bond to prepare the MB/APBA/Ab-HRP and then glucose treatment to obtain MB/APBA/Ab-HRP/GLU. HRP is one of the most extensively studied and commonly used enzymes for the construction of H_2O_2 biosensors. Generally, direct transfer of an electron between HRP and an electrode is difficult because the active sites of HRP are deeply buried in a thick protein shell and because the large distance between the active sites and the electrode surface will slow down the electron transfer. Electron transfer via a mediator like HQ, however, is more effective for establishing an electrical connection between the redox centers and the electrode [20]. In this work, H_2O_2 was a substrate reduced by Ab-HRP, and HQ was used as a mediator for electron transduction. Previously, chorionic gonadotrophin has been proved to decrease the catalytic activity of the Ab-HRP on the detection probe and reduce the current signal on the immunosensor [21]. In another paper, when the antigen of parathyroid hormone increased, the catalytic activity (Kcat) of Ab-HRP on SPCE decreased, and the signal current decreased [17]. These papers suggest the mechanism as follows. When the concentration of antigen increased, the thickness of immuno-complexes on MBs increased. The non-electroactive complex was a blocking layer against the mass transfer of H_2O_2 to HRP sites and also impeded the transfer of the electron mediator HQ to the electrode. EIS is an effective method for probing the features of an electrode using an impedance signal. We also found an increase in the Rct values after the formation of immuno-complexes on MBs when an increase

in spike protein concentrations. This could be ascribed to the formation of the antigen–antibody complex, which could increase the impedance and hinder the transfer of electrons to the electrode. This explained the spike protein concentration was inversely proportional to the current signal.

Characterization of modified MBs

The morphology of modified MBs was investigated by scanning electron microscope (SEM) and transmission electron microscope (TEM) imaging. Figure 2(A–D) shows microscale images of the original MBs and modified MBs with a 1.0 µm scale bar. All images were obtained with 15 kV voltage. MBs are typically sphere shape, as seen in Fig. 2(A); MB/APBA has an aggregated cloud-like structure, as in Fig. 2(B), and MB/APBA/Ab-HRP have expanded clusters, possibly from the interaction of Ab-HRP with increased size, as shown in Fig. 2(C). An aggregated globular structure was observed in Fig. 2(D). In addition, the various sizes of the MBs were characterized using a Zeta sizer. An increase in size from 978 to 1041 nm was indicated the conjugation of APBA on the MB surface. Similarly, after immobilizing Ab-HRP, the size increased to 1535 nm and finally reached 2674 nm after adsorption of spike protein (Table S1). To select MBs, we performed a test with two kinds of MB, one containing the NH_2 group and the other containing the COOH group.

We evaluated HRP adsorption using two kinds of MBs modified by APBA. The crosslinkers tested for $MB-NH_2$ and MB-COOH were glutaraldehyde and EDC/NHC, respectively. We measured the APBA remaining in the solution using UV absorbance at 233 nm. By using the APBA standard as a reference, the concentration of APBA was evaluated and plotted, as in Fig. S2(A). To confirm the effect of

correct orientation, glutaraldehyde is used as a cross-linker to conjugate Ab-HRP to magnetic beads without APBA. The $MB-NH_2$ was directly activated using a glutaraldehyde solution to form $MB-NH_2$/GA. The Ab-HRP was added to the MB-GA and incubated for 30 min, and a TMB assay was used to evaluate the HRP activity of the MBs. Figure S2(B) shows the comparison of the calibration curve of MB with and without the APBA layer. $MB-NH_2$/GA/APBA/Ab-HRP had higher activity (slope) than $MB-NH_2$/GA/Ab-HRP. The APBA can covalently bond to 1,2- and 1,3-diols of the carbohydrate moiety of glycoproteins that can immobilize the Ab-HRP on the MBs. Previously, antibodies were immobilized using their lysine, arginine, and glutamine residues by random conjugation of glutaraldehyde on electrode surfaces, resulting in unsatisfactory activity in antigen targeting [22]. The immobilization of the oriented antibody with the proper targeting activity has been achieved using APBA [23]. Owing to the oriented immobilization of Ab-HRP via boronic acid groups on MB, more activity of the Ab-HRP was preserved in this study. Glutaraldehyde randomly conjugates the Ab-HRP using the amino-acid residues with the amines on $MB-NH_2$, resulting in the decrease of HRP activity. The presence of APBA on the MB surface help to preserve more Ab-HRP activity, as shown in Fig. S2(B). Figure S3(A–D) shows TEM images of the modified MBs. The two MBs ($MB-NH_2$, MB/APBA) had a similar pattern. However, the comparison shows that $MB-NH_2$ looks less aggregated with a smaller size. Upon immobilization, a round aggregated structure with increased size was observed. Antibody immobilization and signal amplification are two key factors in target detection at ultra-low concentrations. The boronic acid in APBA forms cyclic esters with 1,2- and 1,3-diols on the carbohydrate moiety of glycoproteins that can immobilize the antibody on the MBs [24, 25]. APBA
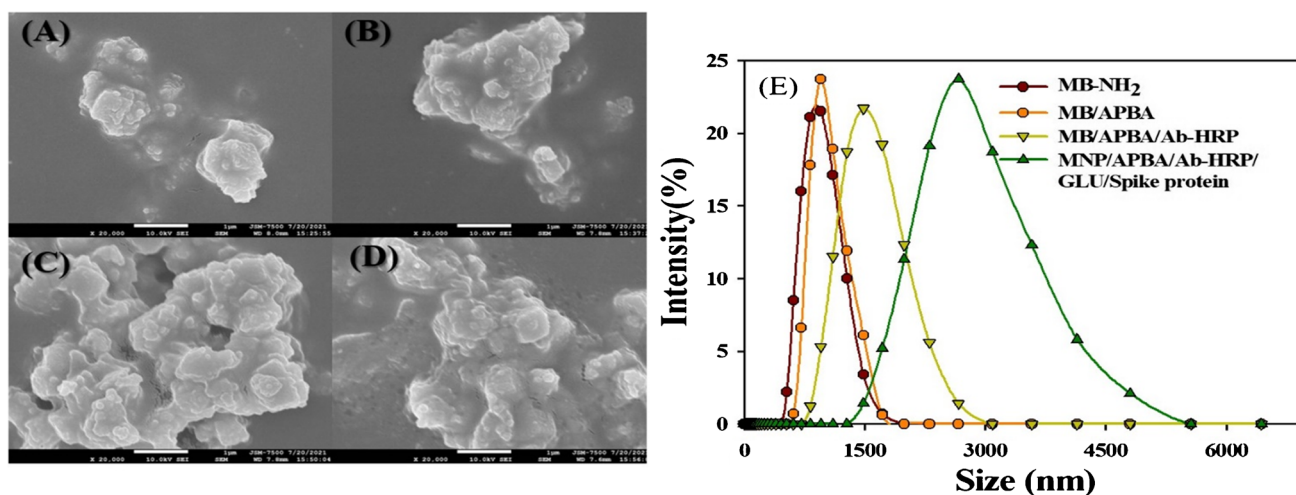

Fig. 2 SEM images of layer-by-layer modified MBs **A** $MB-NH_2$, **B** MB/APBA, **C** MB/APBA/Ab-HRP, **D** MB/APBA/Ab-HRP/GLU/spike protein with scale bar: 1 µm, and **E** size distribution of modified MBs

can maintain the correct antibody orientation and improve antibody targeting efficiency [26]. Therefore, we adopted APBA as a ligand to the immobilized antibody on MB to maintain the correct orientation of antibodies.

The thermal decomposition of MBs was analyzed under a nitrogen atmosphere and a heating rate of 10 °C min $^{-1}$. The TGA result is shown in Fig. 3(A). There are two major endothermic procedures, found at 334 and 380 °C, respectively. The first weight loss region ranging from 61 to 271 °C is responsible for 2% weight loss. The first weight-loss region shall be named as the thermal release of crystal water in MB-APBA. Second weight loss indicates high decomposition temperature, this weight loss region is regarded as the destruction and decomposition of the APBA layer under thermal effect. On the other hand, the TGA analysis

of MB-NH$_2$ showed only one decomposition process, starting at 280 °C. For a further understanding, the magnetic properties of our MB were measured using SQUID. The magnetization curve of MB and MB/APBA were measured and compared in Fig. 3(B).

Electrochemical characterization

EIS has been performed to characterize the stepwise fabrication procedures of this immunosensor, and the effect of electrode modification can be reflected on Rct as reported by Ren et al. [27]. Impedance results during the MB modification are shown in Fig. 4(A). In Fig. 4(B), the MB-free electrode shows the lowest value of Rct ($1238\,\Omega$). After conjugating MB-NH$_2$ with APBA, the Rct value increased
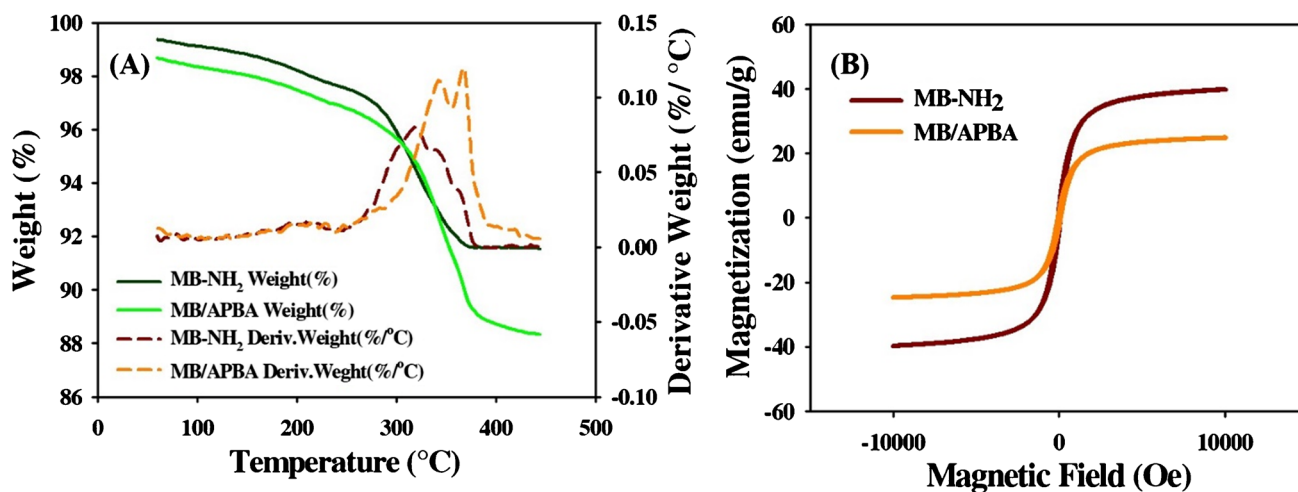

Fig. 3 **A** Thermogravimetric analysis of modified MBs; **B** magnetic hysteresis of MB-NH$_2$ and MB/APBA
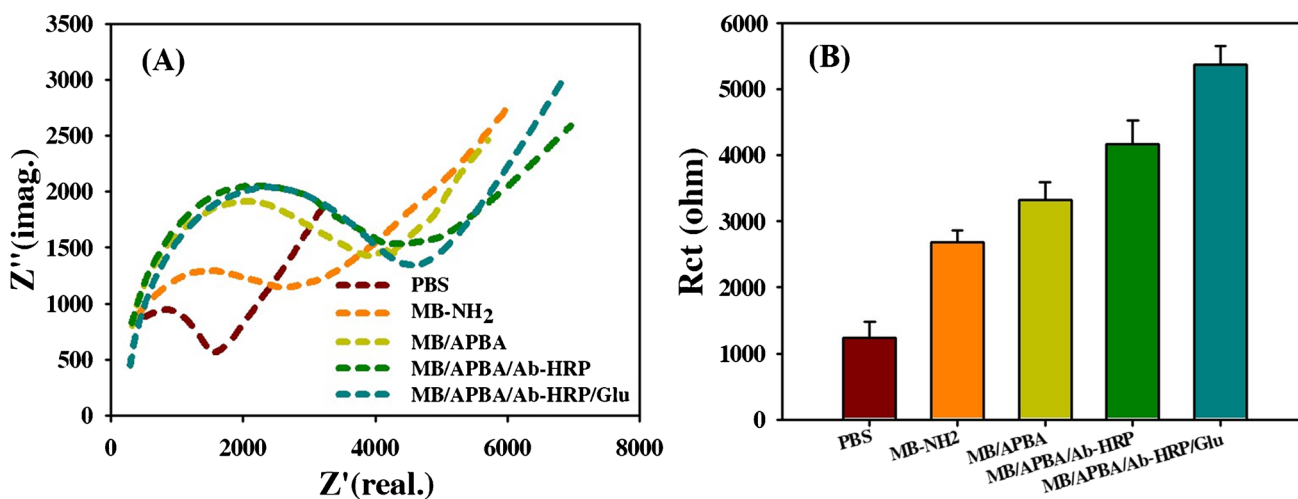

Fig. 4 **A** Impedance results of layer-by-layer modified MBs using 3 mM ferricyanide in phosphate buffer solution. **B** Histogram of charge transfer resistance of modified MBs on bare SPE. Error bar represents the standard deviation from three repeats $n = 3$

to 3316 Ω. Then, there was a significant increase in the Rct value after the antibody was immobilized on the MB surface. After blocking with glucose, the MB/APBA/Ab-HRP/GLU had the highest Rct. The solution resistance and the double-layer capacitance were similar after layer-by-layer modification on MBs, suggesting these parameters were not affected by the APBA conjugation and antibody immobilization [10, 28]. However, Rct values were significantly influenced by the binding of spike protein on MBs. The hindrance to the electron transfer process, blocking of a redox reaction, and the hamper of electron tunneling to the electrode attributed to the increasing thickness of the immuno-complex formed on MB surfaces [29]. EIS is a non-destructive and label-free measurement for the immuno-complex by applying the small amplitude perturbation to collect the impedance information of the electrode.

Thus, Rct results confirmed the successful fabrication of the immunosensor. The kinetic parameters of modified MBs, such as electron transfer rate constant (Ks, cm s^{-1}), were compared after modification (Fig. S4 and Table S2). The oxidation and reduction peak currents in CV from different electrode surfaces can be theoretically attributed to electron transfer rates (Ks) and Rct. The MB-free SPE had higher Ks; upon modification, the values of the Ks decreased. MB-NH$_2$ has a Ks value of 0.19 cm s^{-1}, and upon coating with APBA, the Ks value decreases slightly to 0.18 cm s^{-1}. After Ab-HRP was immobilized, there was a significant decrease in Ks (0.17 cm s^{-1}). Finally, after glucose blocking the value decreased to 0.13 cm s^{-1} as in Fig. S4(B). The reduction of electron transfer rate after the layer-by-layer modification was observed.

Optimization of the experimental parameter

Optimization of HRP and antibody dilution

The antibody, as a sensing element, must have a strong immobilization on the MBs with a good homogenous orientation to detect spike protein efficiently. Moreover, the modified MBs must be stable enough to bear the modification condition and the electrochemical assay. For HRP optimization, various dilution from 50 to 200× was tested. The delta current (ΔI) rose as HRP folds increased to 100× and then decreased. One 100--fold dilution had the highest S/B ratio, as shown in Fig. S5(A). Based on the S/B ratio, 100× HRP was selected as the optimized HRP fold. Similarly, for antibody dilution, different antibody folds (50 to 200× were chosen) and an optimized HRP fold (100×) were selected for this test. The delta current gradually decreased as the antibody fold increased, as noted in Fig. S5(B). The optimized condition for the antibody fold was 100× as it had the highest S/B ratio.

Optimization of incubation time, H$_2$O$_2$/HQ concentration, and blocking process

The effects of incubation time and H$_2$O$_2$/HQ concentration were investigated for sensitive electrochemical detection of COVID-19 spike protein. Given the incubation time of the antibody, immobilization plays a key role in binding with the spike protein. To improve the total assay time, the incubation times of Ab-HRP were tested. To optimize incubation time, 10, 20, 30, and 60 min were tested. The optimized Ab-HRP fold was selected for this test. The SWV signal indicated that 30 min had the highest S/B ratio, as seen in Fig. S5(C). The optimization process led to an incubation period of 30 min for the 100 × dilution HRP and 100 × Ab concentration. Similarly, to optimize the H$_2$O$_2$/HQ concentration, 2.5/2.5, 5/5, 10/10, and 20/20 mM were tested. The delta current (ΔI) was increased with H$_2$O$_2$/HQ concentration, as seen in Fig. S5(D). The highest S/B ratio occurred at 5/5 mM of H$_2$O$_2$/HQ. Therefore, it was selected for further testing.

Previously, boronic acid-functionalized MB (BA-MB) has been reported to isolate immunoglobulin G synthesized by recombinant cells [30]. Glucose has the BA binding ability via the cis-diol linkage and affects the antibody purification by BA-MB. Borlido et al. also demonstrate that glucose can compete the BA on MB with the glycoproteins [31]. Using this concept, we first immobilized the Ab-HRP and sequentially blocked the free APBA binding sites using the optimized glucose concentration to avoid the nonspecific binding from the samples. The blocking process is very crucial for immunosensor preparation because it protects the immobilized antibodies and avoids nonspecific binding of impurities on electrodes. Therefore, six blocking agents were added to the MB surface and evaluated for their ability to prevent nonspecific binding. The chemicals tested included 5% dextran sulfate, bovine serum albumin, phosphate buffer solution, gamma-cyclodextrin, glucose, polyethylene glycol. Based on experimental data, the S/B ratio of glucose was higher than BSA shown in Fig. S6. Therefore, glucose was chosen to block the free APBA on the MB surface. The optimized parameters are summarized in Table 1. In addition, other related parameters, such as the APBA concentration and the incubation time of the spike protein, were tested using a HRP activity assay. The optimized APBA concentration on MBs was 0.1%, and the incubation time of spike protein was found to be 30 min (Fig. S7).

Detection of spike protein

The analytical performance of the MB-based immunosensor was investigated by SWV. The dose–effect of spike protein ranging from 3.12 to 200 ng mL^{-1} was evaluated. We investigated the sensor's ability to detect the spike protein of SARS-CoV-2 added in human saliva, urine, and serum. The

Table 1 Summary of optimization of experimental parameters

Parameter	Test range	S/B results	Chosen setting	Best S/B ratio
HRP fold	50–400×	2.39–3.78	100×	3.78
Ab fold	50–400×	2.78–3.81	100×	3.81
Incubation time (Ab)	10–60 min	2.07–3.82	30 min	3.82
H_2O_2/HQ ratio	2.5/2.5–20/20 mM	2.58–3.83	5/5 mM	3.83
Reaction time of MB	5–20 s	3.16–3.27	5 s	3.27
MB loading volume	1–7 μL	2.60–3.80	5 μL	3.80

*HRP, horseradish peroxidase; *Ab*: antibody; *MB*, magnetic bead; *HQ*, hydroquinone; H_2O_2, hydrogen peroxide

SWV spectra of saliva, urine, and serum samples are shown in Fig. 5(A, B, C), and their standard curves are shown in Fig. 5(D, E, F). The current signal decreased with increasing doses of spike protein because higher concentrations of antigen decreased the current signal of the HRP-labeled antibody. This was because the antigen occupied the limited binding sites of antibody-HRP to form an immunocomplex. The current was inversely proportional to the concentration of spike protein, and there was a linear dependence on spike protein concentrations in the range of 3.12 to 200 ng mL^{-1}. This yielded sensitivities of 4.44, 2.49, and 0.84 μA ng^{-1} mL and LODs of 0.20, 0.31, and 0.54 ng mL^{-1} in human saliva, urine, and serum, respectively. The dose-dependent SWV signals could be explained by Rct results. The thickness of immuno-complexes on MBs increased when the spike protein increased. The inert complex hindered the H_2O_2/HQ reaction with HRP and also reduced the electron transfer of the redox mediator to the SPE. Previous reports also demonstrate the targets of immunosensors decrease the activity of the HRP-labelled antibody on the immunosensor and reduce the current signal [21]. A detailed comparison of LOD is shown in Table S3. The data and recovery of SWV, ELISA, and EIS are summarized in Table 2. The developed MBs can also be applied to the colorimetric assay. In the absence of spike protein, the TMB was converted by MB/APBA/Ab-HRP/GLU and became blue. The dose–effect of spike protein on EIS is shown in Fig. 6(A). The Rct value increases with an increase in the dose of the spike protein. The linear relationship between the concentration of spike protein and the Rct value is shown in Fig. 6(B). Based on the equation, we evaluated the association constant (Ka) and found it to be 4.11 ng^{-1} mL.
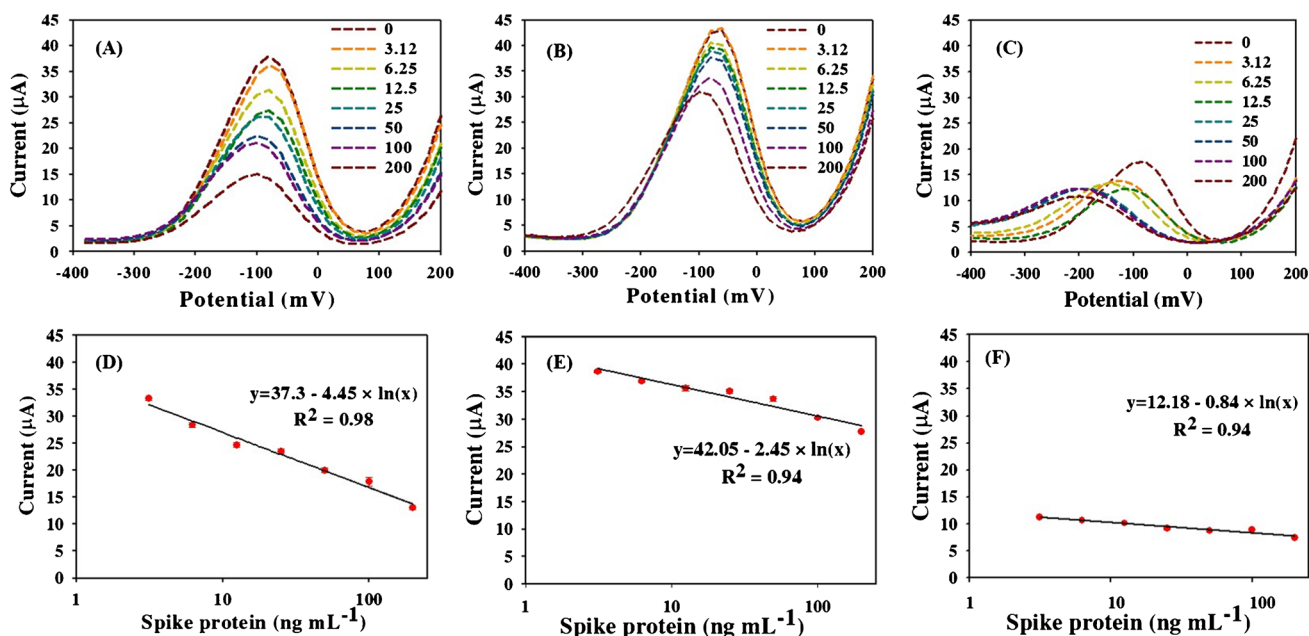

Fig. 5 SWV signals generated from spike protein added in **A** saliva, **B** urine, **C** serum. Calibration curves based on peak currents from spike protein added in **D** saliva, **E** urine, **F** serum using MB-based immunosensors. Detection was carried out on the working surface of SPE by placing an external magnet and loading 5 μL of sample and 95 μL of HQ/H_2O_2. Each data point represents the mean ± SD of three separate measurements were obtained by using the same SPE. The working potential was around 92 mV

Table 2 Comparison of recovery yield of spike protein by EIS, SWV, and ELISA method*

Spike protein (ng mL^{-1})	EIS found (ng mL^{-1})	EIS recovery (%)	SWV found (ng mL^{-1})	SWV recovery (%)	ELISA found (ng mL^{-1})	ELISA recovery (%)
6.25	6.0 ± 0.5	96	7.4 ± 0.5	118	$17.6 \pm 5.6 \times 10^{-3}$	282
12.5	13.2 ± 0.1	105	16.9 ± 0.4	135	$19.3 \pm 2.9 \times 10^{-2}$	154
25	24.6 ± 0.1	98	22.0 ± 0.4	88	$34.3 \pm 1.6 \times 10^{-2}$	137
50	44.3 ± 0.8	88	48.8 ± 0.5	97	$34.3 \pm 1.4 \times 10^{-3}$	68
100	124 ± 2.1	124	77.7 ± 0.8	77	$114.0 \pm 8 \times 10^{-3}$	114
200	179 ± 0.2	90	234 ± 0.3	117	$211.0 \pm 2 \times 10^{-3}$	106

*Recovery $(\%) = \frac{found}{added} \times 100$; *SWV*, square wave voltammetry; *EIS*, electrochemical impedance spectroscopy. The mean $\pm$ standard deviation is from three independent measurements ($n = 3$)

Fig. 6 **A** Impedance results for the measurement of the association constant using spike protein, **B** standard curve of $\triangle R_{CT}(Ci)/R_{CT}(C_0)$ versus spike protein concentration to obtain the associate constant
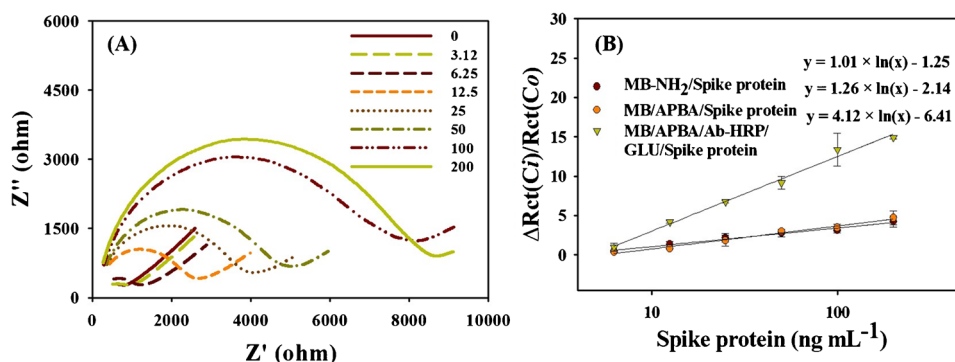
Interference test

To study the selectivity of the fabricated immunosensors, human serum spiked with 10 ng mL^{-1} of spike protein was evaluated in the presence of potentially interfering compounds in serum such as vitamin C, serum albumin, urea, RNase, DNase, trypsin, immunoglobulin, and cell culture medium (DMEM). Spike protein (10 ng mL^{-1}) was used as the positive control for the SWV method. Spike protein had the highest S/B ratio (control). In the presence of an interferent, the MB-based immunosensor still showed a similar current response. Urea and DNase would reduce the signal currents and S/B ratios. The other interferents did not significantly affect the spike protein detection of MB-based immunosensor (Fig. 7).

Stability and storage test

The developed MBs were stored at 4 °C for 49 days to evaluate their storage stability. MB/APBA was treated by Ab-HRP and 5% glucose to freshly prepare MB/APBA/Ab-HRP/GLU. The storage stability of modified MB was evaluated based on the S/B ratio and SWV signal in Fig. 8(A). After 49 days of storage of MB/APBA, the S/B ratio was 3.66, which indicated it has great sensing ability. For MB/

APBA/Ab-HRP/GLU, the S/B ratio on Day 1 was 3.44, and after 49 days of storage, it declined to 2.85. The activity and targeting of antibody-peroxidase on MBs could be retained after 49 days of storage, as shown in Fig. 8(B). More than 80% of the S/B ratio had been maintained as compared with freshly prepared MBs. This suggests that the antibody-immobilized MBs had good stability.

A comparison of the published immunosensors to this study is summarized in Table 3. These reported immunosensors adopted the EIS, DPV, SWV, and CV methods to quantify the targets on SARS-CoV-2. For example, Eissa and Zourob integrated sample collection and detection into a single platform using diazonium-modified SPEs for nucleocapsid detection. They achieved a limit of detection of 0.8 pg mL^{-1} for SARS-CoV-2, and there was no significant cross-reactivity against the influenza antigen [32]. SPEs coated with graphene oxide and gold nanostars can detect the viral spike protein, with a superior limit of detection of 1.68×10^{-22} µg mL^{-1} [33]. In these papers, nanomaterials such as MBs and gold nanoparticles are used to amplify the electrochemical signal using different mechanisms, including a large active surface, extraordinary electron-transfer ability, and multivalent affinity with the enzyme and antibody. Very recently, an electrochemical assay was developed for Nucleocapsid protein using primary antibody-labeled

Fig. 7 SWV histogram of the MB-based immunosensor (MB/APBA/Ab-HRP/GLU) under the interfering compounds. The tested spike protein concentration in human serum was 10 ng mL^{-1}. $n=3$
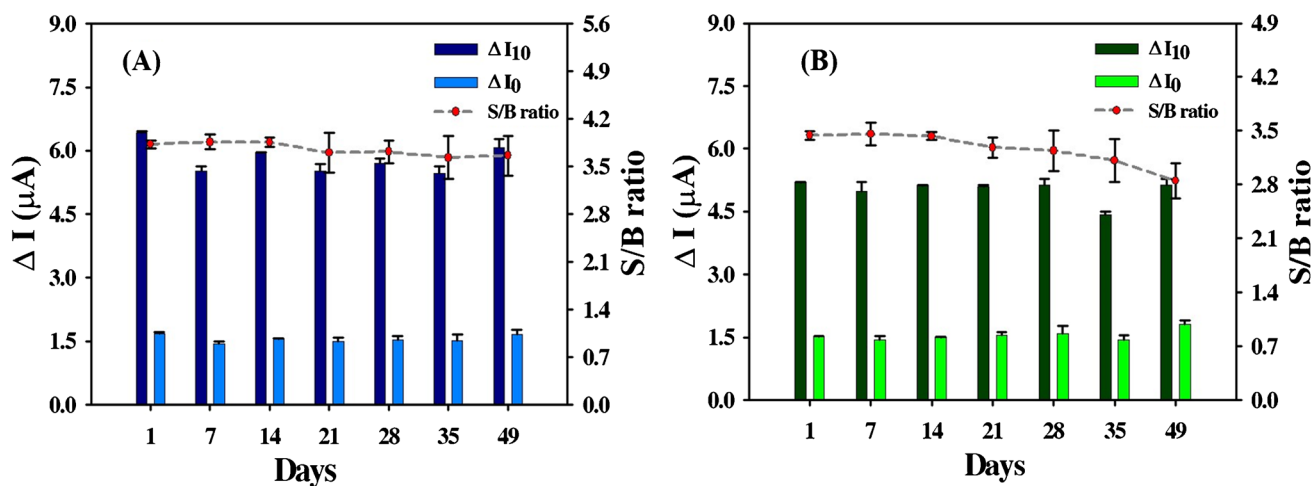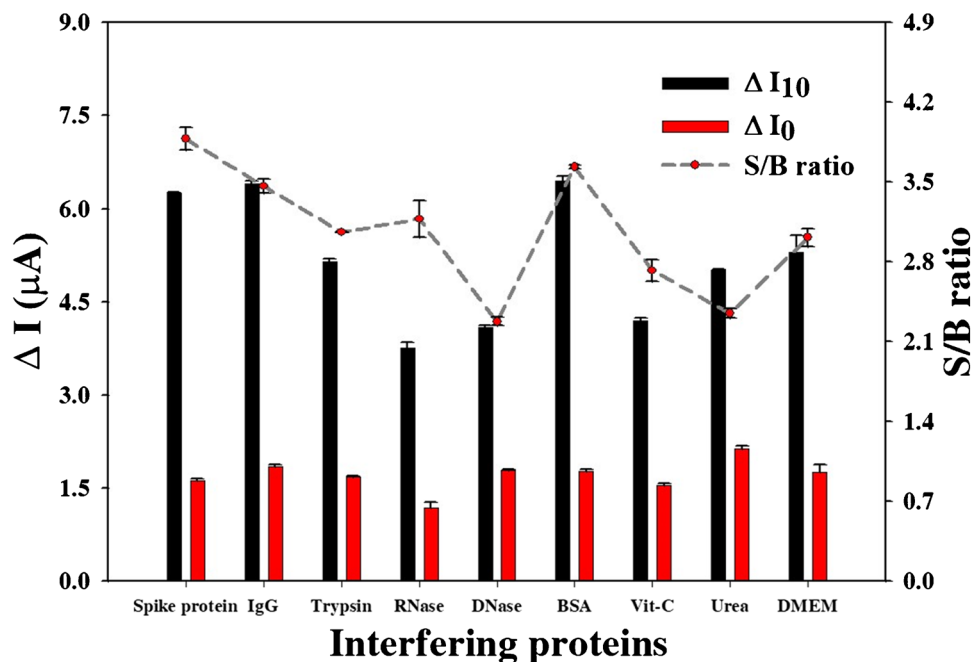

Fig. 8 Stability tests of modified MBs **A** MB/APBA and **B** MB/APBA/Ab-HRP/GLU after 49-day storage at 4 °C. SWV was run with amplitude 75 mV, pulse period 100 mV, and initial potential (200 to −400 mV) using H$_2$O$_2$/HQ. The tested spike protein concentration was 10 ng mL^{-1}

Table 3 Comparison of various nanomaterial-based electrochemical methods for detection of SARS-CoV-2

Nanomaterials/electrode used	Target	Method*	Linear range (ng mL^{-1})	LOD (ng mL^{-1})	Reference
Graphene/carbon electrode	SARS-CoV-2 S protein	EIS	2.5×10^{-7}–1	2.5×10^{-7}	[11]
AuNP-modified SPE	SARS-CoV-2 N protein	SWV	1–10^2	4×10^{-4}	[12]
Diazonium-modified SPE	SARS-CoV-2 N protein	SWV	10^{-3}–10^3	8×10^{-4}	[32]
MB-based SPE	SARS-CoV-2 N protein	SWV	10–10^3	19	[33]
PCB electrode	Amplicons from PCR	DPV	0.1–2×10^2	10	[34]
MB-based SPE	SARS-CoV-2 S protein	SWV	3.12–2×10^2	Saliva: 0.20 Urine: 0.31 Serum: 0.54	This work

*DPV, differential pulse voltammetry; EIS, electrochemical impedance spectroscopy; SWV, square wave voltammetry

MB to capture antigen and secondary antibody-labeled phosphatase to detect antigen and generate enzymatic product naphthol [34]. The carbon black modified SPE then converted the naphthol to the current signal. This novel device of Fabiani et al. provides low LOD and rapid analysis. However, two antibodies and several wash steps were needed as compared to the single antibody and simultaneous detection in the present study. Our proposed MB-based immunosensor could detect spike protein using the SWV and EIS methods with a fast procedure and acceptable sensitivity. However, these following challenges still need to be carefully investigated in future studies. This developed method is limited to the viremia stage, where viruses enter the bloodstream and have access to the rest of the body. Because the clinical samples contain proteins, cells, and biomolecules that can interfere with the selectivity and sensitivity of the developed biosensors, the evaluation using in patient's samples from nasopharyngeal swabs can prove the clinical application of this system. Finally, the antibody used in this study has the limits of being heat sensitive and unstable to long-term storage, which will need further improvement.

Conclusion

We developed a magneto immunosensor for detecting the SARS-CoV-2 spike protein in three body fluids by combining MB-based SPEs and a portable potentiostat. The sensitive and reliable detection was achieved in a label-free format by monitoring the change in the SWV current upon binding with the spike protein. This MB can detect spike protein by electrochemical methods with good stability and reproducibility. This portable device can also be used to confirm the conventional analysis of spike protein by lateral flow and ELISA-like methods. This platform's advantages include low-cost MBs, disposable electrodes, label-free detection, and facile assay in contrast to the expensive PCR instruments. We demonstrated rapid electrochemical analysis of spike protein with an acceptable sensitivity, which has the potential to be used for point-of-care diagnostics.

Declarations

Conflict of interest The authors declare no competing interests.

References

1. Hussein HA, Hassan RYA, Chino M, Febbraio F (2020) Point-of-care diagnostics of covid-19: from current work to future perspectives. Sensors 20(15):1–28. https://doi.org/10.3390/s20154289
2. Rabiee N, Bagherzadeh M, Ghasemi A, Zare H, Ahmadi S, Fatahi Y, Dinarvand R, Rabiee M, Ramakrishna S, Shokouhimehr M, Varma RS (2020) Point-of-use rapid detection of SARS-CoV-2: nanotechnology-enabled solutions for the covid-19 pandemic. Int J Mol Sci 21(14):1–23. https://doi.org/10.3390/ijms21145126
3. Wang C, Liu M, Wang Z, Li S, Deng Y, He N (2021) Point-of-care diagnostics for infectious diseases: from methods to devices. Nano Today 37:101092. https://doi.org/10.1016/j.nantod.2021.101092
4. Khan MZH, Hasan MR, Hossain SI, Ahommed MS, Daizy M (2020) Ultrasensitive detection of pathogenic viruses with electrochemical biosensor: state of the art. Biosens Bioelectron 166:112431. https://doi.org/10.1016/j.bios.2020.112431
5. Eivazzadeh-Keihan R, Pashazadeh-Panahi P, Mahmoudi T, Chenab KK, Baradaran B, Hashemzaei M, Radinekiyan F, Mokhtarzadeh A, Maleki A (2019) Dengue virus: a review on advances in detection and trends – from conventional methods to novel biosensors. Microchim Acta 186(6):329. https://doi.org/10.1007/s00604-019-3420-y
6. Crapnell RD, Banks CE (2021) Electroanalytical overview: utilising micro- and nano-dimensional sized materials in electrochemical-based biosensing platforms. Microchim Acta 188(8):268. https://doi.org/10.1007/s00604-021-04913-y
7. Karakuş E, Erdemir E, Demirbilek N, Liv L (2021) Colorimetric and electrochemical detection of SARS-CoV-2 spike antigen with a gold nanoparticle-based biosensor. Anal Chim Acta 1182:338939. https://doi.org/10.1016/j.aca.2021.338939
8. Kumar MS, Nandeshwar R, Lad SB, Megha K, Mangat M, Butterworth A, Knapp CW, Knapp M, Hoskisson PA, Corrigan DK, Ward AC, Kondabagil K, Tallur S (2021) Electrochemical sensing of SARS-CoV-2 amplicons with PCB electrodes. Sens Actuators, B Chem 343:130169. https://doi.org/10.1016/j.snb.2021.130169
9. Cao L, Xiao H, Fang C, Zhao F, Chen Z (2020) Electrochemical immunosensor based on binary nanoparticles decorated rGO-TEPA as magnetic capture and Au@PtNPs as probe for CEA detection. Microchim Acta 187(10):584. https://doi.org/10.1007/s00604-020-04559-2
10. Pusomjit P, Teengam P, Thepsuparungsikul N, Sanongkiet S, Chailapakul O (2021) Impedimetric determination of cortisol using screen-printed electrode with aptamer-modified magnetic beads. Microchim Acta 188(2):41. https://doi.org/10.1007/s00604-020-04692-y
11. Ehsan MA, Khan SA, Rehman A (2021) Screen-printed graphene/carbon electrodes on paper substrates as impedance sensors for detection of coronavirus in nasopharyngeal fluid samples. Diagnostics 11(6):1030. https://doi.org/10.3390/diagnostics11061030
12. Eissa S, Alhadrami HA, Al-Mozaini M, Hassan AM, Zourob M (2021) Voltammetric-based immunosensor for the detection of SARS-CoV-2 nucleocapsid antigen. Microchim Acta 188(6):199. https://doi.org/10.1007/s00604-021-04867-1
13. Rahmati Z, Roushani M, Hosseini H, Choobin H (2021) Electrochemical immunosensor with Cu(2)O nanocube coating for detection of SARS-CoV-2 spike protein. Microchim Acta 188(3):105. https://doi.org/10.1007/s00604-021-04762-9
14. Povedano E, Gamella M, Torrente-Rodríguez RM, Ruiz-Valdepeñas Montiel V, Montero-Calle A, Solís-Fernández G, Navarro-Villoslada F, Pedrero M, Peláez-García A, Mendiola M, Hardisson D, Feliú J, Barderas R, Pingarrón JM, Campuzano S (2021) Multiplexed magnetic beads-assisted amperometric bioplatforms for global detection of methylations in nucleic acids. Anal Chim Acta 1182:338946. https://doi.org/10.1016/j.aca.2021.338946

15. Cheeveewattanagul N, Guajardo Yévenes CF, Bamrungsap S, Japrung D, Chalermwatanachai T, Siriwan C, Warachit O, Somasundrum M, Surareungchai W, Rijiravanich P (2021) Aptamer-functionalised magnetic particles for highly selective detection of urinary albumin in clinical samples of diabetic nephropathy and other kidney tract disease. Anal Chim Acta 1154:338302. https://doi.org/10.1016/j.aca.2021.338302

16. Malla P, Liao HP, Liu CH, Wu WC (2021) Electrochemical immunoassay for serum parathyroid hormone using screen-printed carbon electrode and magnetic beads. J Electroanal Chem 895:115463. https://doi.org/10.1016/j.jelechem.2021.115463

17. Chen GC, Liu CH, Wu WC (2021) Electrochemical immunosensor for serum parathyroid hormone using voltammetric techniques and a portable simulator. Anal Chim Acta 1143:84–92. https://doi.org/10.1016/j.aca.2020.11.045

18. Sánchez-Paniagua M, Palenzuela-Batista S, Manzanares-Palenzuela CL, López-Ruiz B (2020) Electrochemical genosensor for Klotho detection based on aliphatic and aromatic thiols self-assembled monolayers. Talanta 212:120735. https://doi.org/10.1016/j.talanta.2020.120735

19. Tolan DA, Elshehy EA, El-Said WA, Taketsugu T, Yoshizawa K, El-Nahas AM, Kamali AR, Abdelkader AM (2022) Cubically cage-shaped mesoporous ordered silica for simultaneous visual detection and removal of uranium ions from contaminated seawater. Microchim Acta 189(1):3. https://doi.org/10.1007/s00604-021-05083-7

20. Saleh AJ (2012) Hydrogen peroxide biosensors based on horseradish peroxidase and hemoglobin. J Biosens Bioelectron S9. https://doi.org/10.4172/2155-6210.S9-001

21. Chen J, Tang J, Yan F, Ju H (2006) A gold nanoparticles/sol-gel composite architecture for encapsulation of immunoconjugate for reagentless electrochemical immunoassay. Biomaterials 27(10):2313–2321. https://doi.org/10.1016/j.biomaterials.2005.11.004

22. Park JY, Chang BY, Nam H, Park SM (2008) Selective electrochemical sensing of glycated hemoglobin (HbA1c) on thiophene-3-boronic acid self-assembled monolayer covered gold electrodes. Anal Chem 80(21):8035–8044. https://doi.org/10.1021/ac8010439

23. Lin PC, Chen SH, Wang KY, Chen ML, Adak AK, Hwu JRR, Chen YJ, Lin CC (2009) Fabrication of oriented antibody-conjugated magnetic nanoprobes and their immunoaffinity application. Anal Chem 81(21):8774–8782. https://doi.org/10.1021/ac9012122

24. Cesewski E, Johnson BN (2020) Electrochemical biosensors for pathogen detection. Biosens Bioelectron 159:112214. https://doi.org/10.1016/j.bios.2020.112214

25. Andreev EA, Komkova MA, Nikitina VN, Karyakin AA (2019) Reagentless impedimetric sensors based on aminophenylboronic acids. J Anal Chem 74(2):153–171. https://doi.org/10.1134/S1061934819010040

26. Trilling AK, Beekwilder J, Zuilhof H (2013) Antibody orientation on biosensor surfaces: a minireview. Analyst 138(6):1619. https://doi.org/10.1039/c2an36787d

27. Ren H, Zhang S, Huang Y, Chen Y, Lv L, Dai H (2020) Dual-readout proximity hybridization-regulated and photothermally amplified protein analysis based on MXene nanosheets. Chem Commun 56(87):13413–13416. https://doi.org/10.1039/d0cc05148a

28. Liao BY, Chang CJ, Wang CF, Lu CH, Chen JK (2021) Controlled antibody orientation on Fe3O4 nanoparticles and CdTe quantum dots enhanced sensitivity of a sandwich-structured electrogenerated chemiluminescence immunosensor for the determination of human serum albumin. Sens Actuators, B Chem 336:129710. https://doi.org/10.1016/j.snb.2021.129710

29. Farka Z, Juřík T, Kovář D, Trnková L, Skládal P (2017) Nanoparticle-based immunochemical biosensors and assays: recent advances and challenges. Chem Rev 117(15):9973–10042. https://doi.org/10.1021/acs.chemrev.7b00037

30. Borlido L, Azevedo AM, Roque ACA, Aires-Barros MR (2011) Potential of boronic acid functionalized magnetic particles in the adsorption of human antibodies under mammalian cell culture conditions. J Chromatogr A 1218(43):7821–7827. https://doi.org/10.1016/j.chroma.2011.08.084

31. Borlido L, Azevedo AM, Sousa AG, Oliveira PH, Roque ACA, Aires-Barros MR (2012) Fishing human monoclonal antibodies from a CHO cell supernatant with boronic acid magnetic particles. J Chromatogr B Anal Technol Biomed Life Sci 903:163–170. https://doi.org/10.1016/j.jchromb.2012.07.014

32. Eissa S, Zourob M (2021) Development of a low-cost cotton-tipped electrochemical immunosensor for the detection of SARS-CoV-2. Anal Chem 93(3):1826–1833. https://doi.org/10.1021/acs.analchem.0c04719

33. Hashemi SA, GolabBehbahan NG, Bahrani S, Mousavi SM, Gholami A, Ramakrishna S, Firoozsani M, Moghadami M, Lankarani KB, Omidifar N (2021) Ultra-sensitive viral glycoprotein detection NanoSystem toward accurate tracing SARS-CoV-2 in biological/non-biological media. Biosens Bioelectron 171:112731. https://doi.org/10.1016/j.bios.2020.112731

34. Fabiani L, Saroglia M, Galatà G, De Santis R, Fillo S, Luca V, Faggioni G, D'amore N, Regalbuto E, Salvatori P, Terova G, Moscone D, Lista F, Arduini F (2021) Magnetic beads combined with carbon black-based screen-printed electrodes for COVID-19: a reliable and miniaturized electrochemical immunosensor for SARS-CoV-2 detection in saliva. Biosens Bioelectron 171:112686. https://doi.org/10.1016/j.bios.2020.112686